CHAPTER 3

RESULTS

In this chapter, I will present the results of my calculations. I will begin with the deuteron photodisintegration process in Section 3.1, where I will provide predictions for the cross section (Subsection 3.1.1) and polarization observables (Subsection 3.1.2). Next, in Section 3.2, I will present my predictions for the observables in ^{3}He photodisintegration. Moving on to Section 3.3, I will illuminate the results of calculations for Triton photodisintegration observables. Finally, in Section 3.4, I will discuss the results of the calculations for the pion absorption from the lowest atomic orbital of ^{2}H, ^{3}H, and ^{3}He.

3.1 Deuteron photodisintegraion

3.1.1 Cross section

In this section I will show the results of my calculation starting from the deuteron photodisintegration process. One of the most studying observable is obviously the cross section. There is several papers which present measurement results for both differential and total cross section [1, 66–73] and it is interesting to compare our predictions with that experimental results.

In Fig. 3.1 and Fig. 3.2 I present predictions for the total cross section σ_{tot} [μb] which I obtained using the chiral SMS potential at the N^{4}LO$^+$ order and with the cut-off parameter $\Lambda = 450$ MeV. From Fig. 3.1, we see that at low photon energies (below 50 MeV) both 1NC predictions and results which include 2N contributions to the electromagnetic current via the Siegert approach, describe experimental results quite well quantitatively. We observe that predictions based on the 1NC describe the data only up to approx. 10 MeV. Beyond that energy the 1NC current is clearly not enough to describe cross section as corresponding predictions are clearly below the data. In that region 1NC+Siegert predictions deliver better data description but overestimate the data. The difference between 1NC and 1NC+Siegert cross section grows with increasing photon energies. At 5 MeV the difference between 1NC predictions and 1NC+Siegert is 297.54 µb (10.8 %), increasing energy to 10 MeV it is 304.28 µb (20.4 %) and at 20 MeV it is 229.50 µb (39.2 %).

Here and later the relative difference between a set of predictions $(x_1, x_2, ..., x_N)$ is calculated using the formula:

$$\Delta = \frac{\max(x) - \min(x)}{\frac{1}{N}\sum_{i=1}^{N} x_i} \cdot 100\%, \tag{3.1}$$

so in the specific case of comparison the data with 1NC current and "1NC + Siegert" we calculate the relative difference as $\Delta = \frac{|\sigma^{1NC+Siegert} - \sigma^{1N}|}{0.5(\sigma^{1NC+Siegert} + \sigma^{1N})}$.

From Fig. 3.1 we see that the gap between these predictions continues increasing even more with larger energies. This tells us that the Siegert approach works quite well as when no additional 2N contributions are taken into account. The cross section predictions corrected via Siegert 2N contribution reproduce experimental data to some extent. Fig. 3.1 reveals the approximated character of the Siegert approach. It is clear that one has to take with caution Siegert predictions at very small energies. Also above 20 MeV there is a gap between Siegert results and experimental data, which points that more elaborated 2N current should be included in the future. The observed discrepancy cannot be explained by the cut-off dependence (see e.g. Fig. 3.5b below) or by the low order of chiral potential (see discussion below).

While my main goal is to describe deuteron photodisintegration at energies $E_\gamma \lesssim 50$ MeV, where predictions seem to describe experimental data reasonably well, it is also interesting to check how present theory works at higher energies. Above $E_\gamma = 50$ MeV we can notice that the discrepancy with experimental data is not only quantitative but also qualitative see Fig. 3.2. This starts already above $E_\gamma = 50$ MeV and is especially pronounced at peak around 300 MeV seen in the experimental data from [70] which is not reflected in my predictions. The reason for such discrepancy is most likely coming from the relativistic effects which we do not take into account within this work. It is also confirmed by the calculations in [19], where authors discuss various NN potentials applied to the deuteron photodisintegration. Despite using much simpler models of the nuclear force than those used in this thesis, their predictions, which include some relativistic effects, show that such a peak appears in their predictions.

In Fig. 3.3 I present the total cross-section for the deuteron photodisintegration at three photon energy values: 30, 100 and 140 MeV as a function of the chiral order. Error bars show truncation errors calculated using Eq. 2.85 - 2.88. One can see that the truncation errors are being reduced with each consecutive chiral order. At LO uncertainty is the biggest: 29.46 % at $E_\gamma = 30$ MeV, 29.46 % at $E_\gamma = 100$ MeV and 41.82 % at $E_\gamma = 140$ MeV. At N^{4}LO$^+$ it is hardly visible at the presented scale and amounts up to 1.3 % for each energy(however decreasing with the chiral order). For each energy, the prediction is within the uncertainty range at lower orders. We see that at lower energy σ_{tot} already at NLO reaches valve which remains practically unchanged at higher orders. Contrarily, at two higher energies, contributions from higher orders are necessary to obtain stable predictions up to approx. N^{3}LO.

Figures 3.4 and 3.5 show my predictions for the differential cross section $\frac{d\sigma}{d\Omega}$. In both figures, the top, middle, and bottom row shows predictions at $E_\gamma = 30$, 100 and 140 MeV, respectively. For all predictions, the contributions of the 2N current are taken into account via the Siegert theorem, and unless stated otherwise, I utilize the SMS N^{4}LO$^+$ potential. The left column of Fig. 3.4 shows the predictions obtained at different chiral orders (from LO to N^{4}LO$^+$) and with $\Lambda = 450$ MeV. Looking at the best predictions (N^{4}LO$^+$, $\Lambda = 450$ MeV) for each energy, I conclude that the higher the photon energy, the larger difference between the theoretical predictions and experimental data is. At $E_\gamma = 30$ MeV (top panel) my predictions almost perfectly match the data and the difference is almost always within the tripled experimental uncertainties. Moving to $E_\gamma = 100$ MeV (middle

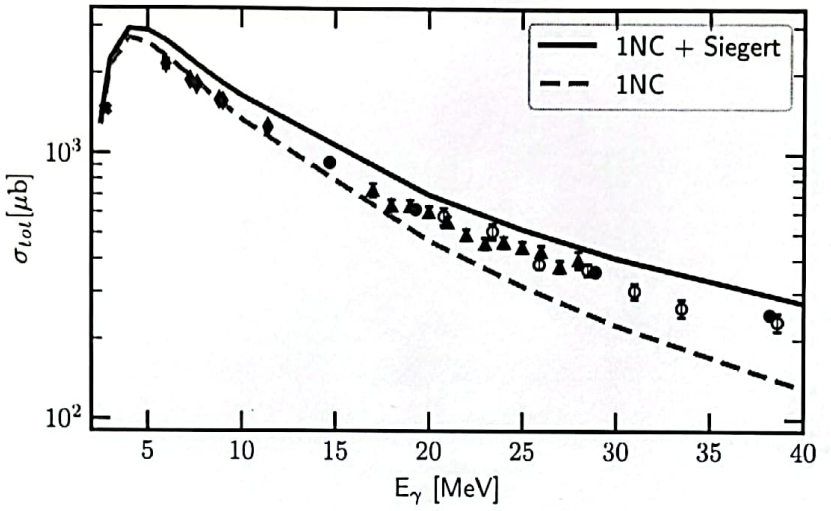

Figure 3.1: Total cross section σ_{tot} for the deuteron photodisintegration process as a function of the photon energy E_γ. The solid blue line presents results obtained with 1NC–Siegert and dashed pink line - predictions based on the 1NC. In both cases the SMS N^4LO^+ $\Lambda = 450\,\mathrm{MeV}$ force is used. The experimental data are from [70] (black filled circles), [66] (empty circles), [1] (triangles), [68] (bold cross "X") and [69] (diamonds).

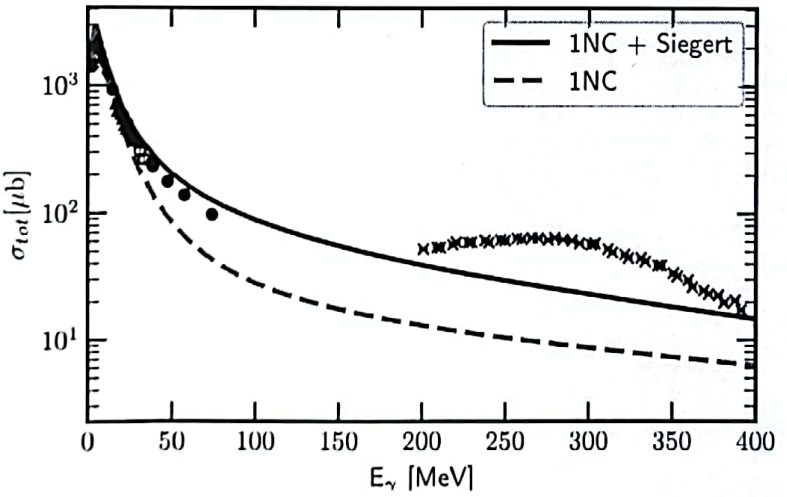

Figure 3.2: The same as in Fig. 3.1 but for the energy range 2.5 - 400 MeV. The experimental data are the same as in Fig. 3.1 but supplemented by the data above $E_\gamma = 200\,\mathrm{MeV}$ from [67] (crosses).

row) the description of the data is deteriorating: theoretical predictions still match the data qualitatively, but the gap for proton emission angle θ_p in range ($60° < \theta_p < 130°$) is up to 32 % (of the predicted value) and relative difference (calculated with Eq. (3.1)) is up to 7 %. At the highest energy (bottom row), it is even hard to say about good qualitative description: the general trend of the angular dependence is presented, but the predictions are far from the experimental points. The relative difference between

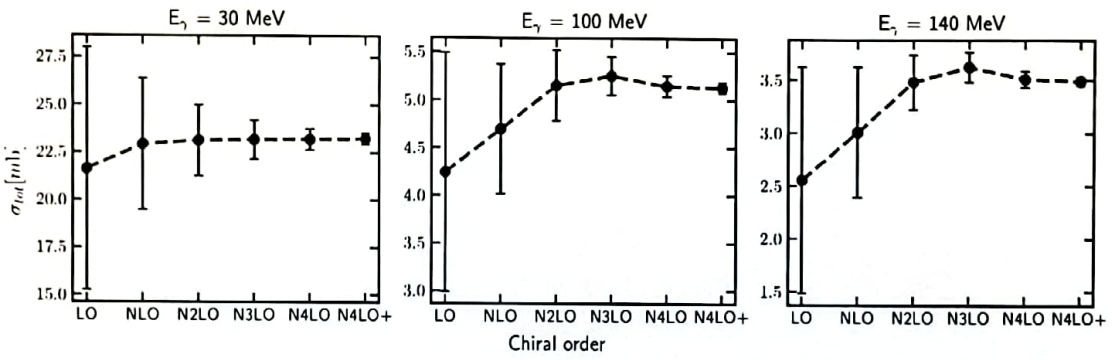

Figure 3.3: Total cross section of the deuteron photodisintegration process as a dependence on the chiral order for three photon energy E_γ values: 30, 100 and 140 MeV. Error bands show an estimated truncation error at each order.

experimental data and predictions obtained with N^4LO+ and $\Lambda = 450$ MeV at 30 MeV is less then 13 % and absolute difference is $< 3.07 \frac{\mu b}{sr}$. At 100 MeV discrepancy is larger and the relative difference reaches 46% with absolute difference up to $1.39 \frac{\mu b}{sr}$. Coming to 140 MeV the relative difference increases up to 48.6 % and absolute - $1.93 \frac{\mu b}{sr}$. What may be helpful for a better data description is a 2N current and relativistic correction mentioned earlier. We observe improvements introduced by each subsequent chiral order, but stabilization shows that some ingredients beyond 2N potential are missing.

The obtained results at each energy confirm the convergence of the predictions concerning the chiral order. We see that the cross section at LO is far from both experimental data and the most advanced N^4LO^+ predictions, and the higher the photon energy, the larger this difference is. With each subsequent chiral order, the curves are more closer to each other and the difference between N^4LO and N^4LO^+ is hardly visible at the scale used in Fig. 3.3. The relative difference between these two predictions at $E_\gamma = 30$ MeV around the point of maximum ($\theta_p = 80°$) is 0.05 % which is $0.02 \frac{\mu b}{sr}$; at 100 MeV and $\theta_p = 107°$ it is 0.79 % ($0.025 \frac{\mu b}{sr}$); and at 140 MeV (same angle) it is 1.8 % ($0.043 \frac{\mu b}{sr}$). Having such small differences between predictions from the two highest chiral orders, I can conclude that predictions are converged and using NN potential beyond N^4LO^+ chiral orders would rather not bring significant contribution to the cross section values. The difference with experimental data is systematic and is not related to the chiral order.

Predictions obtained with the AV18 potential (dashed-dotted purple line in the Fig. 3.4 left) are very similar to these from the N^4LO^+ SMS force at lower energies (relative difference at $E_\gamma = 30$ MeV is 0.06 % at the point of maximum $\theta_p = 80°$) and with increasing energy to 140 MeV it grows up to 3.1 % at the same scattering angle. It can be connected with our potential's quality loss, but AV18 can be struggling with high energies as well. That once again shows that other components of Hamiltonian become important at that energies.

In the right column of the Fig. 3.4 I compare predictions based on various assumptions on nuclear current and dynamical mechanism. I again use SMS N^4LO^+, $\Lambda = 450$ MeV force. At the lowest energy predictions comprising the plane-wave component only (without rescattering part) and taking currents as SNC+Siegert, show relatively small deviation from the full predictions, but the difference increases at larger energies. With $E_\gamma = 30$ MeV the relative difference is 10 % ($4.03 \frac{\mu b}{sr}$) at $\theta_p = 80°$. Difference at 100 MeV and the same angle is 4 % ($0.21 \frac{\mu b}{sr}$) and at 140 MeV it is 7 % ($0.21 \frac{\mu b}{sr}$). In contrast, pre-

dictions without a two-body current component (1NC) have a much larger gap with a full prediction: the difference is 46.5 % (13.67 $\frac{\mu b}{sr}$) at 30 MeV, 78.6 % (2.88 $\frac{\mu b}{sr}$) at 100 MeV and 77.8 % (1.68 $\frac{\mu b}{sr}$) at 140 MeV at the same $\theta_p = 80°$. Obviously, 2NC contributions are extremely important in this case, the difference connected with them is much bigger than theoretical uncertainties or even rescattering contribution. For other scattering angles, especially $\theta_p = 0°$ or $\theta_p = 180°$, the role of two-body current or FSI is relatively even more pronounced.

The Fig. 3.5 (left) presents theoretical truncation uncertainties. That confirms our expectations that for the regarded photoreaction chiral order N^{4}LO$^+$ can produce converged predictions: the black band (representing truncation error at N^{4}LO$^+$) is hardly visible for the $E_\gamma = 30$ MeV (the relative error for N^{4}LO$^+$ at 80° is only 0.12 %) and is also quite narrow for larger energies (at 140 MeV the error at the same angle is 1.46 %). At the lower chiral orders, this band is obviously much wider: at N^{2}LO it is 1.25 % at $E_\gamma = 30$ MeV and 15.0 % at $E_\gamma = 140$ MeV. I note, that the magnitude of the truncation error is only very tiny depending on the scattering angle.

Last but not least, in the right column of Fig. 3.5 I show the cut-off dependence of the differential cross section. In the ideal case, that dependence is so weak that the choice of the parameter Λ would not introduce significant changes. In practice the choice of this parameter is important as it makes a noticeable variation in prediction at higher energies. Namely, ~~while~~ at $E_\gamma = 30$ MeV the cut-off dependence is so tiny that, in fact, all the lines (for different Λ values) overlap each other and we cannot distinguish them with the naked eye: the relative difference at the maximum of the cross section is 0.08 %. This is approximately $\frac{2}{3}$ smaller than the truncation error discussed above. However, with increasing photon energy up to 100 MeV and 140 MeV (middle and bottom rows of the right column of Fig. 3.5) the spread becomes bigger: the uncertainty related to the Λ-dependence is 3.35 % at 100 MeV and 5.66 % at 140 MeV (the same θ_p). Thus at two higher energies, the cut-off dependence becomes more important than truncation errors. That shows, that proper choice of the Λ is important. However, if I restrict myself to $\Lambda = 450$ MeV and 500 MeV, the dependence drops to 1.98 % at $E_\gamma = 140$ MeV. Such a restriction is advocated by a better description of the scattering data delivered by the SMS potential for those two values of Λ.

In the Fig. 2.3 we have already seen that the total cross section for the same energies has the cut-off spread around 4.5 % for 100 MeV and 8 % for 140 MeV For $E_\gamma = 30$ MeV it is below 1 %. It means that ~~even~~ cut-off dependence for that total cross section ~~(affected by the extreme values close to $\theta_p = 0$ or $\theta_p = 180$) are~~ remains relatively small, especially at the lower energies.

Note, that the biggest relative difference arise for regions with θ_p close to 0° or 180°.

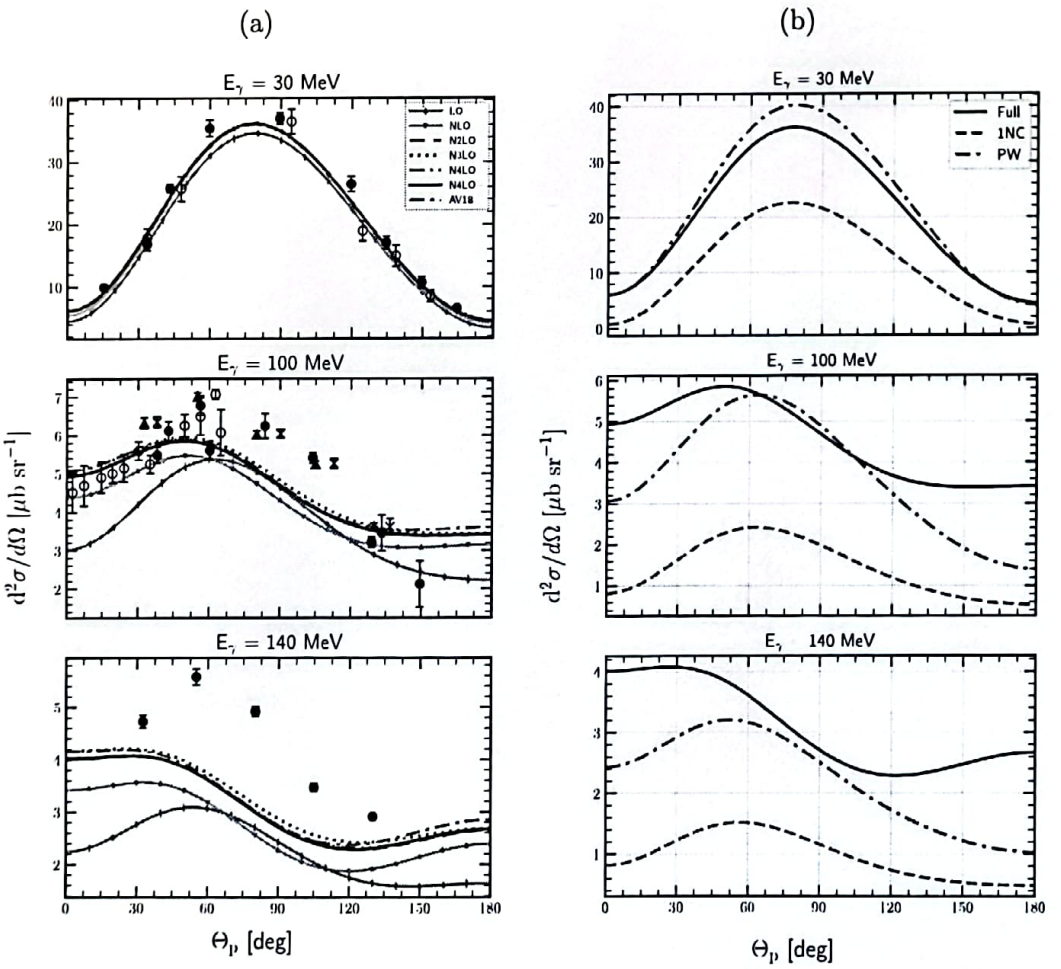

Figure 3.4: Differential cross section $\frac{d^2\sigma}{d\Omega}$ as a function of the outgoing proton momentum polar angle θ_p in the center of mass frame for the photon energy 30 MeV (top), 100 MeV (middle) and 140 MeV (bottom). **(a)** Results obtained using the SMS potential at different chiral orders (from LO to N^{4}LO$^+$) with the cut-off parameter $\Lambda = 450$ MeV and 2NC contributions taken via the Siegert theorem. For the sake of comparison, predictions obtained with the AV18 potential are shown by a dashed-dotted purple line. Data points (filled and empty circles) are from [72] for $E_\gamma = 30$ and 100 MeV and from [73] for $E_\gamma = 140$ MeV. **(b)** Predictions obtained with the chiral N^{4}LO$^+$ potential and $\Lambda = 450$ MeV with various models of nuclear current and scattering state. The blue solid curve represents our most complete predictions comprising the plane-wave plus rescattering parts and 1NC+Siegert current ~~propagator~~ operator (the same as N^{4}LO$^+$ line in (a)). The pink dashed curve shows predictions obtained with the single-nucleon current only (without applying the Siegert theorem) and the green dashed-dotted curve represents predictions with the full current (1NC + Siegert) but plane-wave part only.

(a) Truncation error bands. (b) Cutoff dependence.

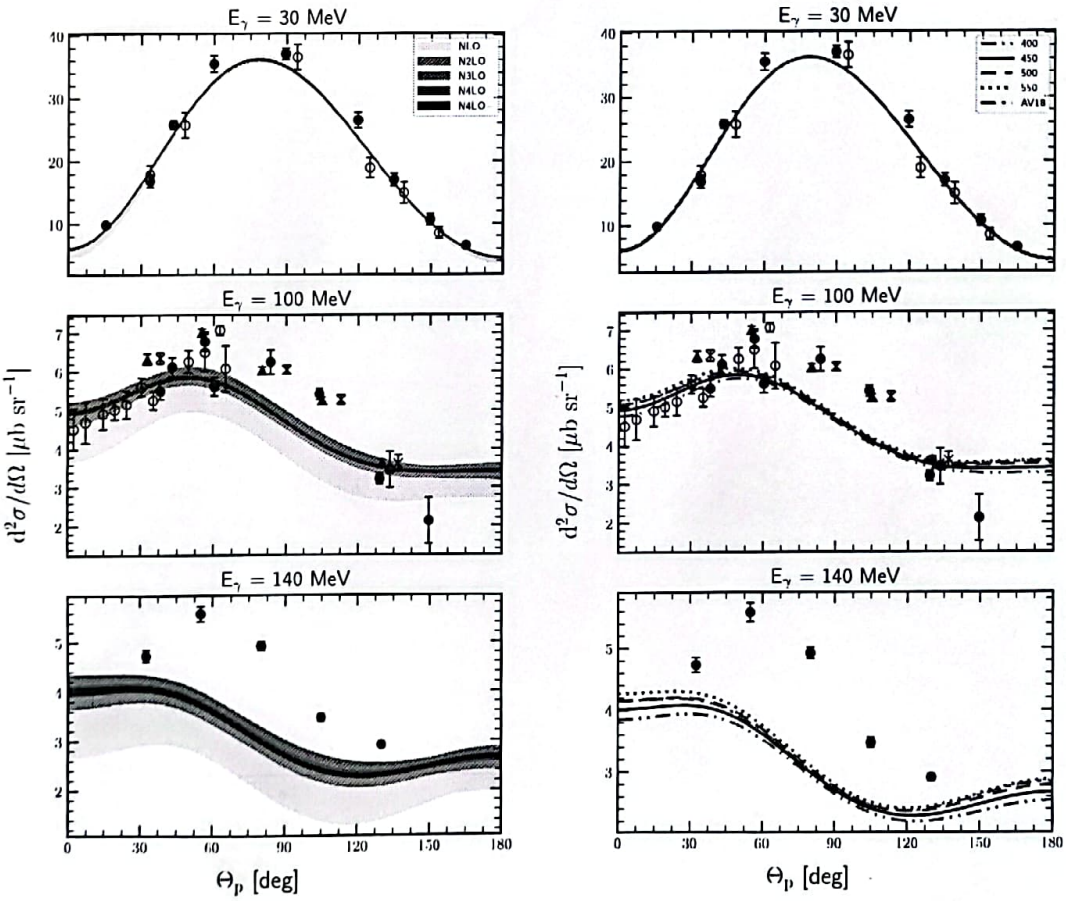

Figure 3.5: Theoretical uncertainties for the differential cross section $\frac{d^2\sigma}{d\Omega}$ as a function of the outgoing proton's momentum polar angle θ_p in the center of the mass frame for the photon energy of 30 MeV (top row), 100 MeV (middle row), and 140 MeV (bottom row). **(a)** The truncation error bands obtained using the SMS potential at different chiral orders (from NLO to N^{4}LO$^+$) with the cut-off parameter $\Lambda = 450$ MeV and 2NC contributions taking via the Siegert approach. **(b)** Results obtained using different values of the cut-off parameter Λ. The double-dotted-dashed red curve, the solid black line, the dashed green line and the dotted blue line represents predictions obtained with $\Lambda =$ 400, 450, 500 and 550 MeV respectively and the chiral potential N^{4}LO$^+$. Data points are the same as in Fig. 3.4a.